HHS Public Access

Author manuscript

Mol Cancer Res. Author manuscript; available in PMC 2023 March 21.

Published in final edited form as:

Mol Cancer Res. 2022 April 01; 20(4): 637–649. doi:10.1158/1541-7786.MCR-21-0402.

KDM6A depletion in breast epithelial cells leads to reduced sensitivity to anticancer agents and increased TGF-β activity

Jin-Fen Xiao[1,2,3,*], **Ley-Fang Kua**[1], **Ling-Wen Ding**[4], **Qiao-Yang Sun**[5], **Khine Nyein Myint**[1], **Xiu-Rong Chia**[1], **Nachiyappan Venkatachalam**[1], **Xinyi Loh**[1], **Jason E. Duex**[6], **Vanessa Neang**[2], **Siqin Zhou**[1], **Ying Li**[1], **Henry Yang**[1], **H. Phillip Koeffler**[1,2], **Dan Theodorescu**[3,6,7,*]

[1]Cancer Science Institute of Singapore, National University of Singapore, Singapore.

[2]Division of Medical Oncology, Cedars-Sinai Medical Center, Los Angeles, CA, USA

[3]Department of Surgery (Urology), Cedars-Sinai Medical Center, Los Angeles, CA, USA

[4]Department of Pathology, Yong Loo Lin School of Medicine, National University of Singapore, Singapore

[5]Department of Hematology, Singapore General Hospital, Singapore

[6]Cedars-Sinai Samuel Oschin Comprehensive Cancer Institute, Los Angeles, CA, USA

[7]Department of Pathology and Laboratory Medicine, Cedars-Sinai Medical Center, Los Angeles, CA, USA

Abstract

KDM6A, an X chromosome-linked histone lysine demethylase, was reported to be frequently mutated in many tumor types including breast and bladder cancer. However, the functional role of KDM6A is not fully understood. Using MCF10A as a model of non-tumorigenic epithelial breast cells, we found that silencing KDM6A promoted cell migration and transformation demonstrated by the formation of tumor-like acini in three-dimensional culture. KDM6A loss reduced the sensitivity of MCF10A cells to therapeutic agents commonly used to treat triple-negative breast cancer patients and also induced TGF-β extracellular secretion leading to suppressed expression of cytotoxic genes in normal human CD8+ T cells *in vitro*. Interestingly, when cells were treated with TGF-β, *de novo* synthesis of KDM6A protein was suppressed while *TGFB1* transcription was enhanced, indicating a TGF-β/KDM6A negative regulatory axis. Furthermore, both KDM6A deficiency and TGF-β treatment promoted disorganized acinar structures in three-dimensional culture, as well as transcriptional profiles associated with epithelial to mesenchymal transition and metastasis, suggesting KDM6A depletion and TGF-β drive tumor progression. Implication: Our study provides the preclinical rationale for evaluating KDM6A and TGF-β in breast tumor

[*]Corresponding authors: Dan Theodorescu, Address: 8700 Beverly Blvd, NT-Plaza Level 2429C, Los Angeles, CA 90048; dan.theodorescu@cshs.org, Phone: +1(310)-423-8431; Jin-Fen Xiao, Address: Davis Research Building RM3057, 110 N George Burns Rd, Los Angeles, CA 90048; jinfen.xiao@cshs.org; Phone: 1(310)423-1326.

CONTRIBUTIONS

J-F.X., D.T., and H.P.K. conceived the experiment and wrote the manuscript. J.E.D. edited the manuscript. J-F.X., L-F.K., L-W. D., Q-Y.S., K.N.M., X-R.C., N.V., X.L., and V.N. performed the experiments. S.Z., Y.L., and H.Y. performed the bioinformatic analysis.

DECLARATION:

J.E.D. receives compensation from Invitae Corporation. All other authors declare no potential conflicts of interest.

samples as predictors for response to chemo and immunotherapy, informing personalized therapy based on these findings.

Keywords

KDM6A; drug resistance; TGF-β; CD8+ T cells; metastasis; epithelial-mesenchymal transition; triple-negative breast cancer

INTRODUCTION

Triple-negative breast cancer (TNBC) lacks expression of estrogen receptor (ER), progesterone receptor (PR), and epidermal growth factor receptor 2 (ERBB2/HER2)[1]. TNBC is commonly diagnosed in premenopausal women and accounts for 15%−20% of all breast cancers[1]. This form of the disease is aggressive and often leads to metastasis and a poor clinical outcome, even when the disease is diagnosed at an early stage[1]. Massive parallel genomic and transcriptomic analysis on patients has shown that TNBC has a high tumor mutation burden (TMB), is highly heterogeneous, and has few actionable driver mutations or signaling pathways[2]. This poses a significant challenge for selecting optimal therapeutic strategies. Currently, agents under clinical investigation in TNBC include inhibitors that target poly ADP ribose polymerase (PARP), phosphoinositide 3-kinase (PI3K), MEK, histone deacetylase (HDAC), androgen and heat shock protein 90 (HSP90)[1]. PARP inhibitors have recently been approved by the U.S. Food and Drug Administration (FDA) for HER2-negative metastatic breast cancer patients with germline BRCA 1/2 mutations, which occurs in 9.7% of TNBC patients[3]. In addition, TNBC exhibits several key characteristics that have been associated with improved response to immunotherapy such as high levels of genomic instability[4], TMB[5], tumor-infiltrating lymphocytes (CD4+, CD8+, and FOXP3+)[6], and expression of programmed cell death 1 ligand (PD-L1)[1]. Immune checkpoint inhibitors combined with chemotherapy have improved progression-free survival and overall survival in patients with advanced or metastatic PD-L1-positive TNBC[7,8] and these combinations are FDA approved for this group. However, significant PD-L1 expression is only present in tumors of 20% of TNBC patients[9], eliminating this therapeutic option for most patients. The remaining patients are offered chemotherapy, which has a moderate response rate and a high probability for relapse[10].

To provide novel mechanistic insights that translate to improved prognostic tools and therapeutic options for TNBC patients, we set out to identify genes that impact aggressiveness and/or drug response. To this end, we developed a novel CRISPR/Cas9 library based on frequently mutated, established, or potential tumor suppressor genes in TNBC. This library was introduced into MCF10A mammary epithelial cells and these cells were used to screen therapeutic agents. MCF10A is a mammary epithelial cell line derived from the fibrocystic tissue of a 36-year-old woman with basal-like transcriptomic and proteomic features of breast cancer and has been widely used in functional genomic screening[11–18]. Our screen discovered that loss of KDM6A expression in MCF10A conferred resistance to several anti-tumor agents and a tumor-like phenotype. Silencing of KDM6A led to TGF-β secretion and impaired CD8+ T cell cytotoxicity *in vitro* while TGF-

β treatment of MCF10A cells decreased KDM6A expression. These observations report for the first time a negative feedback regulatory relationship between TGF-β and KDM6A that may contribute to breast cancer metastasis and resistance to various therapeutic options.

MATERIALS AND METHODS

Cell lines and culture

Hs578T, MDA-MB-231, and BT549 are TNBC subtype breast cancer cell lines and MCF7 is luminal A subtype. MCF10A, Hs578T, and MCF7 cells were purchased from American Type Culture Collection (ATCC). Short tandem repeat (STR) authentication was performed at the Cancer Science Institute of Singapore for validation of cell identity and cells were maintained for <10 passages. MDA-MB-231 and BT549 were purchased from ATCC and generously donated from the lab of Dr. Xiaojiang Cui (Cedars-Sinai)[19]. Mycoplasma was negative in all cell lines (LT07–118, Lonza). MCF10A cells were cultured in DMEM/F12 medium (10565018, Thermo Fisher Scientific) supplemented with 10% horse serum (S090H-500, Biowest), 20 ng/ml epidermal growth factor (EGF, PHG0311L, Life technologies), 0.5 mg/ml hydrocortisone (H0888, Sigma), 100 ng/ml cholera toxin (C8052, Sigma), 10 μg/ml insulin (12585–014, Invitrogen) and 10% Pen/Strep (15140163, Gibco). MDA-MB-231, BT549, and MCF7 cells were cultured with DMEM (12430062, Gibco) supplemented with 10% fetal bovine serum (FBS, 26140079, Gibco). Hs578T was maintained in DMEM supplemented with 10% FBS and 1 μg/ml insulin. Cells were maintained at 37 °C in a humidified incubator under 5% CO_2.

Plasmids

CRISPR plasmids containing single-guide RNA (sgRNA) were generated as previously described[20] using plasmid lentiCRISPRV2 (52961, Addgene). sgRNA sequences for different genes are listed in Supplemental Table S1. shRNA plasmids were generated as described previously[21]. shRNA targeting KDM6A coding region (CDS) (shKDM6A-1) CCGGCCGCGCAAATAGAAATAATTTCTCGAGAAATTATTTCTATTTGCGCGGTTTTTG was generated with lentiviral vector pLKO.1-TRC (10878, Addgene). The shRNA targeting 3'-UTR of KDM6A (shKDM6A-2) was generated with pLKO.1-blast vector (26655, Addgene):CCGGGATTGCACATAGACTAAGAAACTCGAGTTTCTTAGTCTATGTGCAATCTTTTTG. Lentiviral particles were obtained using transfer plasmids including pRSV-Rev, pMDLg/pRRE, and pMD2.G (12253, 12251, and 12259, Addgene) with HEK293FT cells (R70007, Invitrogen).

3D tumor spheroid invasion assay

3D tumor invasion assay was performed as described previously with minor modifications[22]. Detached MCF10A cells (3,000 cells/200 μl culture medium) were seeded in ultra-low attachment 96-well round-bottom plates (7007, Corning). After four days of incubation, tumor spheroids were formed. After removing 150μl of culture medium, Matrigel was dispensed in 1:1 ratio to the culture medium (50 μl) into the U-bottom well. Plates were incubated at 37 °C for 2 hours followed by adding a complete culture medium. Images of

tumor spheroids were taken as a starting point. Images of tumor cells invading Matrigel were taken at 3 and 6 days. Area of invasion was measured using ImageJ software.

Breast acini 3D culture

3D culture for MCF10A acini was performed according to protocols[23] with MCF10A cells growing on top of a thin layer of Matrigel with a diluted 2% Matrigel/medium solution. Briefly, each well of the 8-well chamber slides (30108, SPL Life Science) was overlaid with 50 μl of Matrigel (354234, BD Bioscience), and the slides were incubated at 37°C for 30 minutes to solidify the Matrigel. MCF10A cells were resuspended at 6,250 cells/ml in complete culture medium supplemented with 2% Matrigel. Each well of the pre-coated chamber slide was plated with 400 μl of cells/Matrigel/medium mixture. The slides were incubated in a CO_2 incubator with a change of fresh media every 4 days until day 15. For TGF-β treatment, a complete culture medium with 5 ng/ml TGF-β[24] recombinant protein (CYT-716, Prospec) was added to the chamber slides on day 4 after plating the cells, and fresh media containing 5 ng/ml TGF-β was added every 72 hours today 10. On day 10, the TGF-β containing media was replaced with MCF10A complete medium, and the cultures were incubated for 5 more days.

RNA extraction, qRT-PCR, and RNA-seq

Total RNAs from MCF10A cells were isolated and purified using the RNeasy mini extraction kit (74106, Qiagen). Total RNAs were either sent for RNA-seq analysis or reverse-transcribed to cDNA (K1642, ThermoScientific) and subjected to semi-quantitative PCR reaction (Primers, Supplemental Table S2). Purified RNA was sequenced with the standard Illumina-HiSeq4000 platform, and FASTQ files were analyzed with R (https://www.r-project.org/). Paired-end reads (100 bp) were aligned to GRCh37/hg19. Gene expression was quantified in FPKM units using the DESeq2::fpkm function.

TGF-β enzyme-linked immunosorbent assay (ELISA)

MCF10A cells were seeded to 12-well plates at 5×10^5 cells per well. After 24 hours of culture, the complete culture medium was removed and replaced by 1 ml DMEM/F12 medium without either serum or growth hormone supplement. The serum-free supernatant culture medium was collected at 24, 48, and 72 hours. The concentration of TGF-β in the medium supernatant was examined in triplicate using human TGF-beta 1 ELISA Kit (NBP1–91252, Novus Biologicals) according to the manufacturer's protocol and calculation methods. TGF-β ELISA analysis was performed twice in independent replicates.

T cell activation and treatment

CD8 positive T cells were isolated from commercially available human peripheral blood mononuclear cells (PBMCs) using MACs magnetic bead cell sorting (Miltenyi Biotec.) and activated with 0.25 μg/ml antiCD3ϵ human recombinant proteins (Prospec). The activated T cells were cultured in the conditioned media (supernatant) from either non-targeted control (sgCtrl) or KDM6A-silenced (sgKDM6A) MCF10A cells for 24 hours. For the collection of conditioned media, one million MCF10A sgCtrl and sgKDM6A cells were seeded in 6-well plates for one day before being cultured with 1.5 ml DMEM/F12 media without either

serum or growth hormone supplements. Cells were maintained in culture for 72 hours, and the conditioned media were collected and centrifuged to remove cell debris before treating activated T cells. Twenty microliters of the conditioned media were used to perform the ELISA assay. Activated T cells were also treated with 2.5 ng/ml TGF-β in DMEM/F12 without either serum or growth hormone supplement for 24 hours as described previously[25].

Flow cytometry analysis

T cells cultured in different condition media were harvested and fixed with Fixation Buffer (420801, BioLegend) and permeabilized with Permeabilization Wash Buffer (421002, BioLegend). Staining was performed with the following fluorochrome-conjugated antibodies (1:50) for 30 minutes at 4 °C: FITC-conjugated anti-Granzyme B, PE-conjugated anti-IFN-γ or APC-conjugated anti-perforin (Miltenyi Biotec). A minimum of 10,000 live events was collected in duplicate using BD LSR-II analyzer, and data were analyzed with FlowJo software.

Metabolic labeling and *de novo* KDM6A protein synthesis

MCF10A cells were incubated with or without 5 ng/ml TGF-β for 3 days. Cells were washed twice with warm PBS and incubated in methionine-free DMEM (21013024, Gibco) with 10% dialyzed fetal bovine serum (A3382001, Gibco) with or without TGF-β for 1 hour. For labeling, L-azidohomoalanine (Click-IT AHA, C10102, Thermo Fisher) was added to a final concentration of 50 μM and incubated for 1 hour. Cells were washed twice with chilled PBS, harvested, and lysed with lysis buffer [1% Sodium Dodecyl Sulfate (SDS), 10mM EDTA, and 50mM Tris, pH 8.1] supplemented with protease inhibitor (PI78429, Thermo Fisher) and phosphatase inhibitor (PI78420, Thermo Fisher). After centrifugation at 14,000 RPM for 10 minutes, 1% Triton X-100 and 150 mM NaCl were added to the whole cell lysate and protein concentration was determined using Pierce BCA Protein Assay Kit (23225, Thermo Fisher). The same amount of bulk protein (3 mg) from lysate was used for the detection of newly synthesized KDM6A protein. Immunoprecipitation was carried out with KDM6A antibody (0.5 μg, A302–374A, Bethyl laboratory) for 16 hours. Click reaction to conjugate biotin to immunoprecipitations and input whole-cell extract was performed with biotin alkyne (B10185, Thermo Fisher) using Click-IT reaction buffer kit (C10276, Thermo Fisher) according to manufacturer instructions. Metabolic labeling of AHA to *de novo* KDM6A protein and bulk protein was detected using NeutrAvidin horseradish peroxidase conjugate kit (A2664, Thermo Fisher) and KDM6A antibody (sc-514859, Santa Cruz).

Statistical analysis

Statistical analysis was performed in R statistical computing language (v3.6.3) and GraphPad Prism version 8. Data were presented as mean ± S.D. A two-side student *t*-test was performed for comparing two groups. Pearson correlation and Fisher's exact test were carried out for correlation of two RNA-seq data. A hypergeometric test was performed for calculating the significance of the overlap of two RNA-seq data sets. Statistical significance was defined as p-value < 0.05 for all statistical tests.

Data availability

The raw RNA-Seq data were deposited in the NCBI Gene Expression Omnibus database (GEO GSE131701).

RESULTS

Loss of KDM6A promotes MCF10A resistance to multiple anti-tumor agents

We developed a novel screening platform to study the interaction between the loss of specific gene expression and response to a panel of small molecules (Figure 1A). To establish a list of genes for the screening platform, we interrogated three large breast cancer sequencing databases (TCGA[26], MSK[27], and METABRIC[28]), text-searched in the PubMed database, and analyzed in-house MCF10A RNA-seq data[29]. From this analysis, a list of 58 established/potential tumor suppressor genes in TNBC was selected (see Supplemental Figure S1 for detailed gene list and selection details). We successfully knocked down 32 of these genes, each in an individual MFC10A cell line, as validated by Sanger sequencing (Figure 1B, Supplemental Figure S2A, and Supplemental Table S3) and/or reduced gene expression via immunoblot (Figure 1C and Supplemental Figure S2B). Immunoblots showed that protein expression was absent in some (CBFB, RUNX1, CDH1, SMARCB1, and LNK), while in others it was reduced (KDM6A, ZFP36L1, CHD4, MED12, FANCA, SMAD4, GATA3, ATRX, RB1, and EP300; Figure 1C and Supplemental Figure S2B).

To study the effect of CRISPR/Cas9-induced mutagenesis in response to anti-cancer agents, the 32 cell lines were pooled in even ratios before drug treatment (Supplemental Figure S2C) and exposed to various doses (10 nM to 3 μM) of 42 compounds which are frequently used to treat TNBC and are in pre-clinical or clinical development (Phase I-III trials) or FDA approved (Figure. 1D and see also Supplemental Tables S4 and S5). These 42 consists of chemotherapeutic agents and a wide range of targeted inhibitors, such as inhibitors for a receptor tyrosine kinase (RTK), HDAC, PARP, AKT, and others (Figure 1E and Supplemental Tables S4 and S5). Next, we compared the normalized frequency of each sgRNA in drug-treated versus mock controls after 5 days of cell growth. This allowed us to assess the enrichment or loss of specific sgRNA cell populations in response to drug treatment. This in turn enabled us to predict the effect that loss of the probable tumor suppressor genes has on tumor response to anti-tumor agents (Figure 1F). Silencing these 32 probable tumor suppressors with targeted sgRNA had only minimal to moderate effect on proliferation of MCF10A cells after 5 days treatment with DMSO, relative to the corresponding starting-point control (control sgRNA, Supplemental Figure S2D). In contrast, in the presence of multiple drugs, the sgRNA targeting KDM6A exhibited a consistently increased frequency compared to the corresponding mock control (Figure 1F). Thus, silencing KDM6A led to increased resistance to multiple agents, an observation that has not been previously reported. KDM6A is an X-linked histone demethylase that antagonizes the enzymatic activity of the methylase EZH2 by specifically demethylating di- and tri-methylated H3 lysine 27 (repressive histone modifications to gene expression)[30–32]. We validated the drug screen sensitivity by demonstrating that silencing of KDM6A conferred MCF10A resistance to paclitaxel (cytotoxic chemotherapy), AZD2014 (mTOR inhibitor), and dasatinib (RTK inhibitor) (Figure 1G and Supplemental Figure S2E).

MCF10A cells acquire tumor-like characteristics with KDM6A loss

KDM6A is commonly mutated in multiple cancer types, including gastric[33], urothelial[34], pancreatic[35], and breast[36,37]. KDM6A is a tumor suppressor gene with most mutations predicted or shown to be loss-of-function[35,38]. Since the functional impact of such changes on cancer phenotypes such as growth, migration, invasion, and drug resistance are not completely characterized[39–41], we sought to investigate KDM6A using breast cancer as a model. MTT and BrdU incorporation assays showed that CRISPR-mediated silencing of KDM6A had little effect on cell proliferation of MCF10A (Figures 2A, and 2B, supplemental Figure S2D). In contrast, the Boyden chamber transwell assay showed the migratory ability of MCF10A cells significantly increased after KDM6A silencing (Figure. 2C) consistent with the previous reports[40]. To measure the invasive capacity of MCF10A cells after silencing of KDM6A, a three-dimensional/3D-spheroid multicellular assay was employed. Loss of KDM6A allowed the multicellular spheroids of MCF10A to grow in the Matrigel-embedded anchorage-independent setting, which was not observed in non-targeted control cells (Figure. 2D). We also discovered that silencing of KDM6A led to reduced E-cadherin and higher expression of Vimentin (Figure. 2E), supporting that KDM6A loss leads to a more mesenchymal, motile, and invasive phenotype. Next, we examined the impact of KDM6A depletion on the formation of acinar hollow structures seen in non-transformed cells (Figure. 2F)[42] and found this to lead to luminal filling and progressive irregular multiacinar enlargement (Figures 2G and 2H).

KDM6A loss promotes *TGFB1/TGFB2* transcription and TGF-β signaling

To begin delineating the molecular mechanism underlying the above observations, RNA-seq was carried out on cells with KDM6A depletion (Figure. 3A). This identified significant upregulation of 599 genes and downregulation of 547 genes (Figure. 3B). Gene ontology (GO) and pathway analysis [KEGG, NetPath, Wikipathways, and Reactome (supplemental Figure S3)] showed enrichment of cancer metastasis-related processes/pathways: focal adhesion, cell migration, gap junction, and extracellular matrix organization (Figure 3C and Supplemental Figure S3). Notably, TGF-β receptor and signaling pathways were enriched, which are major drivers of epithelial to mesenchymal transition (EMT) and cancer metastasis[43], as well as regulators of PI3K/AKT/mTOR and IL-10 signaling[44] (Figure 3C). Supporting our biological observations in cells with silenced KDM6A, gene set enrichment analysis (GSEA) identified cohorts of genes involved in invasion, EMT, and response to TGF-β stimulation (Figure 3D). In addition, we found a significant correlation between luminal to mesenchymal transition, EZH2 targets, stem cells, and stromal stimulation signatures that occurred with reduced KDM6A expression (Figure 3D), as previously noted[40,45]. We also observed decreased expression of genes related to tight-junction, upregulation of genes involving metastasis, inflammation, and TGF-β signaling (Figure 3E). Taken together, there is a strong correlation between loss of KDM6A and increases in signatures related to metastasis and TGF-β signaling.

Loss of KDM6A leads to the secretion of TGF-β and suppression of CD8+ T cell activity

Next, we used qRT-PCR to confirm the mRNA expression of key genes found in the transcriptional profiling (Figure 4A). Since TGF-β is secreted into the extracellular matrix

as an inactivated latent complex[46] and activation of TGF-β requires release from the latency associated peptide[46], we used an ELISA assay to measure the mature TGF-β on conditioned culture media collected from KDM6A-silenced and control cells. TGF-β levels increased over time in conditioned media from KDM6A-silenced MCF10A cells compared to control cells (Figure 4B). Importantly, after 72 hours of incubation, the concentration of TGF-β was high (1.1 ng/ml) and comparable to the elevated plasma levels (2.4 ng/ml) found in breast cancer patients[47,48], which has been associated with disease progression and decreased survival of metastatic breast cancer patients.

Activated TGF-β is known to repress specific genes in cytotoxic CD8+ T cells such as perforin, granzyme B, and interferon-gamma (IFN-γ), which ultimately leads to a reduced capability of lymphocytes to kill tumor cells[25]. To confirm TGF-β secreted from KDM6A-silenced MCF10A cells could suppress CD8+ T cell activity, peripheral blood mononuclear cells from healthy individuals were treated with conditioned media from KDM6A-silenced MCF10A cells, control cells, or recombinant TGF-β. Conditioned media from cells with KDM6A depletion was confirmed to contain elevated levels of TGF-β (Figure 4C) and found to suppress perforin, granzyme B, and IFN-γ expression in CD8+ T cells (Figures 4D and 4E). This reduction was comparable to that seen with recombinant TGF-β (Figures 4D and 4E) and consistent with levels previously shown to impair cytotoxic T cell functions[25].

To evaluate if our observations are generalizable, we examined the impact of KDM6A depletion in other breast cancer cells. Loss of KDM6A in MDA-MB-231, Hs578T, BT549, and MCF7 (Figure 4F) led to upregulation of both *TGFB1* and *TGFB2* (Figure 4G). Of note, all TNBC subtypes (MDA-MB-231, Hs578T, and BT549) and luminal A subtype MCF7 cells showed an increase in *TGFB1* and *TGFB1* mRNA (Figure 4G).

KDM6A expression was reduced by TGF-β

MCF10A cells treated with TGF-β are a model for EMT *in vitro* studies[24] and these cells are resistant to the anti-proliferation effect of TGF-β[24]. A previous report noted that TGF-β suppressed KDM6A protein expression in MCF10A cells, and its expression was restored after TGF-β[41] withdrawal. Here we show that treating MCF10A, as well as MDA-MB-231, Hs578T, BT549, and MCF7 cells, with 5ng/ml TGF-β for 3 days suppressed KDM6A protein expression (Figures 5A and 5B). Supporting a possible mechanistic link between these two molecules was our finding that TGF-β treatment resulted in the transformation of tumor-like acini from MCF10A cells, which phenocopied downregulation of KDM6A expression (Figures 2H and 5C).

Interestingly, mRNA levels of *KDM6A* were not altered after TGF-β treatment (supplemental Figures S4A and S4B). mRNA stability analysis showed that the rate of KDM6A mRNA decay was unaltered after 3 days of TGF-β treatment (Figure 5D), while KDM6A protein levels were significantly reduced (Figures 5A). This suggests that the TGF-β-induced decrease of KDM6A protein levels is post-transcriptional. To examine this hypothesis, a short pulse metabolic labeling experiment with L-azidohomoalanine (AHA) was carried out on MCF10A cells treated with either mock or TGF-β for 3 days. Total KDM6A protein was purified with KDM6A antibody from cell lysate of either control or TGF-β-treated MCF10A cells and biotin-AHA immunoblotting revealed only *de novo*

synthesized KDM6A protein. This examination showed that TGF-β treatment strongly suppressed nascent KDM6A protein synthesis (Figure 5E), supporting our hypothesis that the TGF-β-induced decrease in KDM6A protein levels is post-transcriptional.

Our results are also supported by the breast cancer patient proteome data retrieved from the Clinical Proteomic Tumor Analysis Consortium (CPTAC)[49] which showed a negative correlation between protein levels of TGF-β and KDM6A (Figure 5F). This correlation was observed in all molecular subtypes of breast cancer patients (Figure 5F).

Gene expression signatures and pathway analysis from KDM6A-silenced MCF10A cells mirror those of TGF-β treatment of MCF10A cells

Our results suggested TGF-β treatment triggers similar effects as those observed with KDM6A-loss. To test this hypothesis, we compared the transcriptional response of MCF10A cells to TGF-β treatment [GSE89152, TGF-β (5 ng/ml) treatment 6-day vs. 0-day[24]] to our RNA-seq data from cells loss of KDM6A expression (Figure 3B). A positive correlation was observed between the differentially expressed genes from the two transcriptional profiles (Supplemental Figure S5A). Further analysis showed a significant number of differentially expressed genes (1602 genes) were overlapping between the two data sets (Figure 6A). Pathway analysis of those 1602 genes showed enriched pathways for focal adhesion, extracellular matrix organization, and TGF-β signaling (Figure 6B). Evaluation of genes as a function of KDM6A-silencing (group 1) and TGF-β-treatment (group 2) showed that most pathways enriched in both groups were similar (supplemental Figures. S5B and S5C). Analysis of TGF-β-treated MCF10A cells also showed gene signature enrichment for invasion, EMT, TGF-β signaling, EZH2 targets, stem cells, and stromal stimulation (Figure 6C). These were known gene signatures associated with TGF-β in breast cancer and similar to what we observed in KDM6A-silenced MCF10A cells (Figures 3D and 6C). Likewise, TGF-β treatment of MCF10A, MDA-MB-231, Hs578T, BT549, and MCF7 cells also increased transcription levels of *TGFB1* and *TGFB2* (Figures 6D and 6E). Our results showed that TGF-β treatment resembled KDM6A-loss in regulating its gene transcription, suggesting a TGF-β/KDM6A negative feedback loop.

DISCUSSION

Malignant cellular transformation gives cells the capability to actively invade, metastasize and evade immune surveillance, and these functions are often driven by different molecular alterations[50]. For example, in breast cancer models such as MCF10A, genes such as *ERBB2* and *SRC* (SRC Proto-Oncogene) disrupt acinar structure by both inhibiting apoptosis and filling the lumen structure, while genes like *CCND1* and $PIK3CA^{H1040R}$, although potent drivers of cell proliferation, are insufficient as a single factor to destroy the highly organized acinar structure[51–53]. Our study found that while suppression of KDM6A expression did not affect cell proliferation and tumor growth *in vivo*, loss of KDM6A did enable spheroids of MCF10A cells to proliferate in anchorage-independent Matrigel and disrupt mammary acinar structure with the filling of luminal space, indicating the acquisition of tumor-like characteristics[54]. These observations were in line with a report in mice with KDM6A deletion in mammary epithelium[55]. The absence of KDM6A protein in these mice led to the

abnormal mammary epithelium, conversion of the mammary cell luminal lineage to basal characteristics, and disrupted normal ducts and alveoli structure[55]. These are commonly observed preceding malignant transformation of luminal cells[56]. In these KDM6A-deleted mice, breast cancer was not reported[55]. Collectively, these data do support the notion that KDM6A is an important suppressor of the sequence of events leading to breast malignant transformation.

Reduced KDM6A expression in MCF10A cells resulted in enriched gene signatures for EMT/metastasis, cancer stem cells, and the TGF-β pathway. These are known to be associated with resistance to anti-tumor therapies in breast cancer[57], which may account for the broad spectrum of drug resistance observed in our drug screening results. In addition, our findings relating to EMT and cancer stem cell signatures are consistent with those of others using murine models where KDM6A expression levels are lower in poorly differentiated breast basal/mesenchymal cells than well-differentiated luminal cells[55]. We observed that silencing of KDM6A in MCF10A cells resulted in upregulated transcription of both *TGFB1* and *TGFB2*, as well as secretion of TGF-β protein. TGF-β is a pleiotropic cytokine signaling through SMAD-dependent and independent pathways in cellular homeostasis[58]. TGF-β can function as either a tumor-suppressor or oncogenic driver and this is highly context-dependent during cancer progression. When acting as a tumor suppressor, TGF-β induces cell-cycle arrest and apoptosis via upregulating expression of P16, P21, and apoptotic death-associated protein kinase[58,59]. However, with disease progression and loss of tumor suppressor genes such as P16 and P21 in cancer cells, TGF-β induces epithelial to mesenchymal transition (EMT), enriches cancer stem cells, and drives cancer metastasis[46,58,59]. TGF-β is relevant in breast cancer as it is enriched in the tumor microenvironment and it is a known contributor to breast cancer metastasis[60], breast cancer stem cell proliferation[61], and chemotherapy resistance[62]. Moreover, TGF-β also contributes to epigenetic modifications in breast cancer. However, the regulatory effect of TGF-β in epigenetic regulation is broad and unspecific. TGF-β has been reported to increase both transcriptionally activating (H3R2me1/2[63], H3K4me2/3[64], and H3K27Ac[65]) and suppressing (H3K9me2/3[66] and H3K27me3[67,68]) histone modifications, as well as DNA methylations by regulating different epigenetic regulators. Based on these studies and our results, secreted TGF-β because of KDM6A silencing may be able to modify the epigenome of MCF10A and breast cancer cells through autocrine and/or paracrine signaling. Nonetheless, we observed that secreted TGF-β suppressed expression of cytotoxic genes in CD8+ T cells *in vitro*, which have a negative impact on T cell surveillance[25,69]. We also demonstrated that TGF-β treatment suppressed *de novo* KDM6A protein synthesis post-transcriptionally and led to a transcriptomic profile associated with reduced KDM6A expression. We generalized our findings by showing that TGF-β treatment suppressed KDM6A protein expression in both TNBC (MDA-MB-231, BT549, and Hs578T) and luminal A (MCF7) subtype breast cancer cell lines. In agreement with our cell line results, we also showed that there was a strong negative correlation between protein levels of TGF-β and KDM6A in proteomic data of breast cancer patients. This negative correlation extended beyond TNBC breast cancer patients to three other breast cancer molecular subtypes.

In summary, our observations suggest that KDM6A and TGF-β are partners in a negative feedback regulatory loop that may contribute to therapeutic resistance and escape of

immunosurveillance. Our findings also suggest that suppressing TGF-β may functionally "restore" KDM6A and provide a rationale for exploring inhibition of TGF-β in combination with other anti-tumor agents in breast cancer patients. For example, evaluation of KDM6A and TGF-β in breast tumor samples could be used as predictors for response to chemo and immunotherapy and such findings could subsequently drive personalized therapy.

Supplementary Material

Refer to Web version on PubMed Central for supplementary material.

ACKNOWLEDGEMENT

This research was supported by the National Research Foundation Singapore under its Singapore Translational Research (STaR) Investigator Award (NMRC/STaR/0021/2014) and administered by the Singapore Ministry of Health's National Medical Research Council (NMRC), the NMRC Centre Grant awarded to the National University Cancer Institute of Singapore (NMRC/CG/012/2013 and CGAug16M005), the National Research Foundation Singapore and the Singapore Ministry of Education under its Research Centers of Excellence initiatives. This work was funded by the NCIS Yong Siew Yoon Research Grant through donations from the Yong Loo Lin Trust. This work was also supported by the Michele and Ted Kaplan Family Senior Investigator Grant from the Tower Cancer Research Foundation. Additionally, this work was supported by NIH grant CA075115 to D.T.

REFERENCES

1. Bianchini G, Balko JM, Mayer IA, Sanders ME & Gianni L Triple-negative breast cancer: challenges and opportunities of a heterogeneous disease. Nat Rev Clin Oncol 13, 674–690, doi:10.1038/nrclinonc.2016.66 (2016). [PubMed: 27184417]
2. Ciriello G et al. Comprehensive Molecular Portraits of Invasive Lobular Breast Cancer. Cell 163, 506–519, doi:10.1016/j.cell.2015.09.033 (2015). [PubMed: 26451490]
3. O'Shaughnessy J et al. Prevalence of germline BRCA mutations in HER2-negative metastatic breast cancer: global results from the real-world, observational BREAKOUT study. Breast Cancer Res 22, 114, doi:10.1186/s13058-020-01349-9 (2020). [PubMed: 33109210]
4. Curtis C et al. The genomic and transcriptomic architecture of 2,000 breast tumours reveals novel subgroups. Nature 486, 346–352, doi:10.1038/nature10983 (2012). [PubMed: 22522925]
5. Liu Z, Li M, Jiang Z & Wang X A Comprehensive Immunologic Portrait of Triple-Negative Breast Cancer. Transl Oncol 11, 311–329, doi:10.1016/j.tranon.2018.01.011 (2018). [PubMed: 29413765]
6. Gao G, Wang Z, Qu X & Zhang Z Prognostic value of tumor-infiltrating lymphocytes in patients with triple-negative breast cancer: a systematic review and meta-analysis. BMC Cancer 20, 179, doi:10.1186/s12885-020-6668-z (2020). [PubMed: 32131780]
7. Cortes J et al. Pembrolizumab plus chemotherapy versus placebo plus chemotherapy for previously untreated locally recurrent inoperable or metastatic triple-negative breast cancer (KEYNOTE-355): a randomised, placebo-controlled, double-blind, phase 3 clinical trial. Lancet 396, 1817–1828, doi:10.1016/S0140-6736(20)32531-9 (2020). [PubMed: 33278935]
8. Schmid P et al. Atezolizumab and Nab-Paclitaxel in Advanced Triple-Negative Breast Cancer. N Engl J Med 379, 2108–2121, doi:10.1056/NEJMoa1809615 (2018). [PubMed: 30345906]
9. Mittendorf EA et al. PD-L1 expression in triple-negative breast cancer. Cancer Immunol Res 2, 361–370, doi:10.1158/2326-6066.CIR-13-0127 (2014). [PubMed: 24764583]
10. Lebert JM, Lester R, Powell E, Seal M & McCarthy J Advances in the systemic treatment of triple-negative breast cancer. Curr Oncol 25, S142–S150, doi:10.3747/co.25.3954 (2018). [PubMed: 29910657]
11. Soule HD et al. Isolation and characterization of a spontaneously immortalized human breast epithelial cell line, MCF-10. Cancer Res 50, 6075–6086 (1990). [PubMed: 1975513]
12. Neve RM et al. A collection of breast cancer cell lines for the study of functionally distinct cancer subtypes. Cancer Cell 10, 515–527, doi:10.1016/j.ccr.2006.10.008 (2006). [PubMed: 17157791]

13. Lawrence RT et al. The proteomic landscape of triple-negative breast cancer. Cell Rep 11, 630–644, doi:10.1016/j.celrep.2015.03.050 (2015). [PubMed: 25892236]
14. Martins MM et al. Linking tumor mutations to drug responses via a quantitative chemical-genetic interaction map. Cancer Discov 5, 154–167, doi:10.1158/2159-8290.CD-14-0552 (2015). [PubMed: 25501949]
15. Niepel M et al. A Multi-center Study on the Reproducibility of Drug-Response Assays in Mammalian Cell Lines. Cell Syst 9, 35–48 e35, doi:10.1016/j.cels.2019.06.005 (2019). [PubMed: 31302153]
16. Martinko AJ et al. Targeting RAS-driven human cancer cells with antibodies to upregulated and essential cell-surface proteins. Elife 7, doi:10.7554/eLife.31098 (2018).
17. Ng PK et al. Systematic Functional Annotation of Somatic Mutations in Cancer. Cancer Cell 33, 450–462 e410, doi:10.1016/j.ccell.2018.01.021 (2018). [PubMed: 29533785]
18. Peck B et al. 3D Functional Genomics Screens Identify CREBBP as a Targetable Driver in Aggressive Triple-Negative Breast Cancer. Cancer Res 81, 847–859, doi:10.1158/0008-5472.CAN-20-1822 (2021). [PubMed: 33509944]
19. Han B et al. FOXC1-induced non-canonical WNT5A-MMP7 signaling regulates invasiveness in triple-negative breast cancer. Oncogene 37, 1399–1408, doi:10.1038/s41388-017-0021-2 (2018). [PubMed: 29249801]
20. Shalem O et al. Genome-scale CRISPR-Cas9 knockout screening in human cells. Science 343, 84–87, doi:10.1126/science.1247005 (2014). [PubMed: 24336571]
21. Xiao JF et al. The c-MYC-BMI1 axis is essential for SETDB1-mediated breast tumourigenesis. J Pathol, doi:10.1002/path.5126 (2018).
22. Vinci M, Box C & Eccles SA Three-dimensional (3D) tumor spheroid invasion assay. J Vis Exp, e52686, doi:10.3791/52686 (2015). [PubMed: 25993495]
23. Lee GY, Kenny PA, Lee EH & Bissell MJ Three-dimensional culture models of normal and malignant breast epithelial cells. Nat Methods 4, 359–365, doi:10.1038/nmeth1015 (2007). [PubMed: 17396127]
24. Comaills V et al. Genomic Instability Is Induced by Persistent Proliferation of Cells Undergoing Epithelial-to-Mesenchymal Transition. Cell Rep 17, 2632–2647, doi:10.1016/j.celrep.2016.11.022 (2016). [PubMed: 27926867]
25. Thomas DA & Massague J TGF-beta directly targets cytotoxic T cell functions during tumor evasion of immune surveillance. Cancer Cell 8, 369–380, doi:10.1016/j.ccr.2005.10.012 (2005). [PubMed: 16286245]
26. Hoadley KA et al. Cell-of-Origin Patterns Dominate the Molecular Classification of 10,000 Tumors from 33 Types of Cancer. Cell 173, 291–304 e296, doi:10.1016/j.cell.2018.03.022 (2018). [PubMed: 29625048]
27. Razavi P et al. The Genomic Landscape of Endocrine-Resistant Advanced Breast Cancers. Cancer Cell 34, 427–438 e426, doi:10.1016/j.ccell.2018.08.008 (2018). [PubMed: 30205045]
28. Pereira B et al. The somatic mutation profiles of 2,433 breast cancers refines their genomic and transcriptomic landscapes. Nat Commun 7, 11479, doi:10.1038/ncomms11479 (2016). [PubMed: 27161491]
29. Guo X et al. ARID1A and CEBPalpha cooperatively inhibit UCA1 transcription in breast cancer. Oncogene 37, 5939–5951, doi:10.1038/s41388-018-0371-4 (2018). [PubMed: 29980791]
30. Agger K et al. UTX and JMJD3 are histone H3K27 demethylases involved in HOX gene regulation and development. Nature 449, 731–734, doi:10.1038/nature06145 (2007). [PubMed: 17713478]
31. Hong S et al. Identification of JmjC domain-containing UTX and JMJD3 as histone H3 lysine 27 demethylases. Proc Natl Acad Sci U S A 104, 18439–18444, doi:10.1073/pnas.0707292104 (2007). [PubMed: 18003914]
32. Lee MG et al. Demethylation of H3K27 regulates polycomb recruitment and H2A ubiquitination. Science 318, 447–450, doi:10.1126/science.1149042 (2007). [PubMed: 17761849]
33. Rokutan H et al. Comprehensive mutation profiling of mucinous gastric carcinoma. J Pathol 240, 137–148, doi:10.1002/path.4761 (2016). [PubMed: 27313181]

34. Nickerson ML et al. Concurrent alterations in TERT, KDM6A, and the BRCA pathway in bladder cancer. Clin Cancer Res 20, 4935–4948, doi:10.1158/1078-0432.CCR-14-0330 (2014). [PubMed: 25225064]
35. Andricovich J et al. Loss of KDM6A Activates Super-Enhancers to Induce Gender-Specific Squamous-like Pancreatic Cancer and Confers Sensitivity to BET Inhibitors. Cancer Cell 33, 512–526 e518, doi:10.1016/j.ccell.2018.02.003 (2018). [PubMed: 29533787]
36. van Haaften G et al. Somatic mutations of the histone H3K27 demethylase gene UTX in human cancer. Nat Genet 41, 521–523, doi:10.1038/ng.349 (2009). [PubMed: 19330029]
37. Wang L & Shilatifard A UTX Mutations in Human Cancer. Cancer Cell 35, 168–176, doi:10.1016/j.ccell.2019.01.001 (2019). [PubMed: 30753822]
38. Ezponda T et al. UTX/KDM6A Loss Enhances the Malignant Phenotype of Multiple Myeloma and Sensitizes Cells to EZH2 inhibition. Cell Rep 21, 628–640, doi:10.1016/j.celrep.2017.09.078 (2017). [PubMed: 29045832]
39. Xie G et al. UTX promotes hormonally responsive breast carcinogenesis through feed-forward transcription regulation with estrogen receptor. Oncogene 36, 5497–5511, doi:10.1038/onc.2017.157 (2017). [PubMed: 28534508]
40. Choi HJ et al. UTX inhibits EMT-induced breast CSC properties by epigenetic repression of EMT genes in cooperation with LSD1 and HDAC1. EMBO Rep 16, 1288–1298, doi:10.15252/embr.201540244 (2015). [PubMed: 26303947]
41. Taube JH et al. The H3K27me3-demethylase KDM6A is suppressed in breast cancer stem-like cells, and enables the resolution of bivalency during the mesenchymal-epithelial transition. Oncotarget 8, 65548–65565, doi:10.18632/oncotarget.19214 (2017). [PubMed: 29029452]
42. Bissell MJ, Rizki A & Mian IS Tissue architecture: the ultimate regulator of breast epithelial function. Curr Opin Cell Biol 15, 753–762 (2003). [PubMed: 14644202]
43. Padua D & Massague J Roles of TGFbeta in metastasis. Cell Res 19, 89–102, doi:10.1038/cr.2008.316 (2009). [PubMed: 19050696]
44. Guo X & Wang XF Signaling cross-talk between TGF-beta/BMP and other pathways. Cell Res 19, 71–88, doi:10.1038/cr.2008.302 (2009). [PubMed: 19002158]
45. Ler LD et al. Loss of tumor suppressor KDM6A amplifies PRC2-regulated transcriptional repression in bladder cancer and can be targeted through inhibition of EZH2. Sci Transl Med 9, doi:10.1126/scitranslmed.aai8312 (2017).
46. Moses H & Barcellos-Hoff MH TGF-beta biology in mammary development and breast cancer. Cold Spring Harb Perspect Biol 3, a003277, doi:10.1101/cshperspect.a003277 (2011). [PubMed: 20810549]
47. Ivanovic V et al. Elevated plasma levels of transforming growth factor-beta 1 (TGF-beta 1) in patients with advanced breast cancer: association with disease progression. Eur J Cancer 39, 454–461, doi:10.1016/s0959-8049(02)00502-6 (2003). [PubMed: 12751375]
48. Ivanovic V et al. Elevated plasma TGF-beta1 levels correlate with decreased survival of metastatic breast cancer patients. Clin Chim Acta 371, 191–193, doi:10.1016/j.cca.2006.02.027 (2006). [PubMed: 16650397]
49. Mertins P et al. Proteogenomics connects somatic mutations to signalling in breast cancer. Nature 534, 55–62, doi:10.1038/nature18003 (2016). [PubMed: 27251275]
50. Hanahan D & Weinberg RA Hallmarks of cancer: the next generation. Cell 144, 646–674, doi:10.1016/j.cell.2011.02.013 (2011). [PubMed: 21376230]
51. Debnath J et al. The role of apoptosis in creating and maintaining luminal space within normal and oncogene-expressing mammary acini. Cell 111, 29–40, doi:10.1016/s0092-8674(02)01001-2 (2002). [PubMed: 12372298]
52. Kalkat M et al. MYC Protein Interactome Profiling Reveals Functionally Distinct Regions that Cooperate to Drive Tumorigenesis. Mol Cell 72, 836–848 e837, doi:10.1016/j.molcel.2018.09.031 (2018). [PubMed: 30415952]
53. Bennett HL, Brummer T, Jeanes A, Yap AS & Daly RJ Gab2 and Src co-operate in human mammary epithelial cells to promote growth factor independence and disruption of acinar morphogenesis. Oncogene 27, 2693–2704, doi:10.1038/sj.onc.1210928 (2008). [PubMed: 17998934]

54. Imbalzano KM, Tatarkova I, Imbalzano AN & Nickerson JA Increasingly transformed MCF-10A cells have a progressively tumor-like phenotype in three-dimensional basement membrane culture. Cancer Cell Int 9, 7, doi:10.1186/1475-2867-9-7 (2009). [PubMed: 19291318]
55. Yoo KH et al. Histone Demethylase KDM6A Controls the Mammary Luminal Lineage through Enzyme-Independent Mechanisms. Mol Cell Biol 36, 2108–2120, doi:10.1128/MCB.00089-16 (2016). [PubMed: 27215382]
56. Hein SM et al. Luminal epithelial cells within the mammary gland can produce basal cells upon oncogenic stress. Oncogene 35, 1461–1467, doi:10.1038/onc.2015.206 (2016). [PubMed: 26096929]
57. Brown JA et al. TGF-beta-Induced Quiescence Mediates Chemoresistance of Tumor-Propagating Cells in Squamous Cell Carcinoma. Cell Stem Cell 21, 650–664 e658, doi:10.1016/j.stem.2017.10.001 (2017). [PubMed: 29100014]
58. Massague J TGFbeta in Cancer. Cell 134, 215–230, doi:10.1016/j.cell.2008.07.001 (2008). [PubMed: 18662538]
59. Yeh HW, Lee SS, Chang CY, Lang YD & Jou YS A New Switch for TGFbeta in Cancer. Cancer Res 79, 3797–3805, doi:10.1158/0008-5472.CAN-18-2019 (2019). [PubMed: 31300476]
60. Imamura T, Hikita A & Inoue Y The roles of TGF-beta signaling in carcinogenesis and breast cancer metastasis. Breast Cancer 19, 118–124, doi:10.1007/s12282-011-0321-2 (2012). [PubMed: 22139728]
61. Asiedu MK, Ingle JN, Behrens MD, Radisky DC & Knutson KL TGFbeta/TNF(alpha)-mediated epithelial-mesenchymal transition generates breast cancer stem cells with a claudin-low phenotype. Cancer Res 71, 4707–4719, doi:10.1158/0008-5472.CAN-10-4554 (2011). [PubMed: 21555371]
62. Bhola NE et al. TGF-beta inhibition enhances chemotherapy action against triple-negative breast cancer. J Clin Invest 123, 1348–1358, doi:10.1172/JCI65416 (2013). [PubMed: 23391723]
63. Chen H, Lorton B, Gupta V & Shechter D A TGFbeta-PRMT5-MEP50 axis regulates cancer cell invasion through histone H3 and H4 arginine methylation coupled transcriptional activation and repression. Oncogene 36, 373–386, doi:10.1038/onc.2016.205 (2017). [PubMed: 27270440]
64. Yamamoto S et al. JARID1B is a luminal lineage-driving oncogene in breast cancer. Cancer Cell 25, 762–777, doi:10.1016/j.ccr.2014.04.024 (2014). [PubMed: 24937458]
65. Tufegdzic Vidakovic A et al. Context-Specific Effects of TGF-beta/SMAD3 in Cancer Are Modulated by the Epigenome. Cell Rep 13, 2480–2490, doi:10.1016/j.celrep.2015.11.040 (2015). [PubMed: 26686634]
66. Du D et al. Smad3-mediated recruitment of the methyltransferase SETDB1/ESET controls Snail1 expression and epithelial-mesenchymal transition. EMBO Rep 19, 135–155, doi:10.15252/embr.201744250 (2018). [PubMed: 29233829]
67. Rivero S, Ceballos-Chavez M, Bhattacharya SS & Reyes JC HMG20A is required for SNAI1-mediated epithelial to mesenchymal transition. Oncogene 34, 5264–5276, doi:10.1038/onc.2014.446 (2015). [PubMed: 25639869]
68. Lu C et al. Coordination between TGF-beta cellular signaling and epigenetic regulation during epithelial to mesenchymal transition. Epigenetics Chromatin 12, 11, doi:10.1186/s13072-019-0256-y (2019). [PubMed: 30736855]
69. Gunderson AJ et al. TGFbeta suppresses CD8(+) T cell expression of CXCR3 and tumor trafficking. Nat Commun 11, 1749, doi:10.1038/s41467-020-15404-8 (2020). [PubMed: 32273499]
70. Schmeichel KL & Bissell MJ Modeling tissue-specific signaling and organ function in three dimensions. J Cell Sci 116, 2377–2388, doi:10.1242/jcs.00503 (2003). [PubMed: 12766184]
71. Gaiko-Shcherbak A et al. The Acinar Cage: Basement Membranes Determine Molecule Exchange and Mechanical Stability of Human Breast Cell Acini. PLoS One 10, e0145174, doi:10.1371/journal.pone.0145174 (2015). [PubMed: 26674091]
72. Kenny PA et al. The morphologies of breast cancer cell lines in three-dimensional assays correlate with their profiles of gene expression. Mol Oncol 1, 84–96, doi:10.1016/j.molonc.2007.02.004 (2007). [PubMed: 18516279]

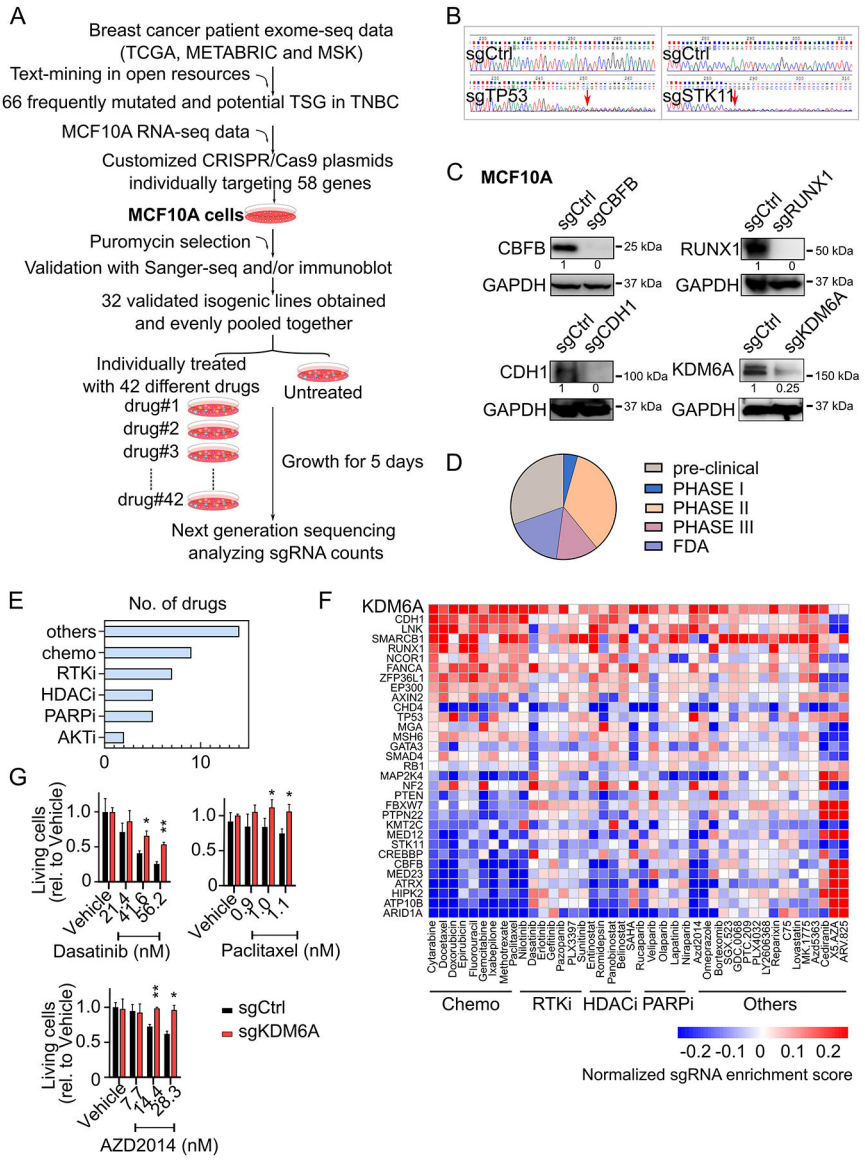

Figure 1. Loss of KDM6A renders MCF10A cells resistant to multiple anti-tumor agents

(A). An overview on the design of a customized CRISPR library and establishment of 32 validated MCF10A isogenic cell lines for drug screening followed by next generation sequencing [see also supplemental Figure S1 for detailed gene selection strategies for picking potential tumor suppressor genes (TSGs) in TNBC]. (B). Tracings of Sanger sequencing mutations produced by sgRNA-directed CRISPR/Cas9 at *TP53* (sgTP53) and *STK11* (sgSTK11). sgCtrl, non-targeted sgRNA control. (C). Western blot examining silencing of CBFB (sgCBFB), RUNX1 (sgRUNX1), CDH1 (sgCDH1) and KDM6A (sgKDM6A) expression after CRISPR-sgRNA. Band intensities were quantified and normalized to GAPDH levels. (D). Pie chart showing the clinical status of the 42 compounds used in this study which include pre-clinical, phase I, II, and III as well as FDA-approved drugs. (E). Distribution of the 42 drugs includes chemotherapeutic agents (chemo) and specific inhibitors: receptor kinase inhibitors (RTKi); HDAC inhibitor (HDACi); PARP

inhibitor (PARPi); AKT inhibitor (AKTi) and others. (F). Heatmap showing response of 32 validated MCF10A isogenic cell lines treated for 5 days with 42 individual anti-tumor agents according to doses shown in Supplemental Table S3. Color bar shows the normalized CRISPR guide enrichment score $\log_2^{\text{sgRNA\_counts (drug treatment/mock control),}}$ which reflects the population of cells carrying specific sgRNA treated with anti-tumor compounds in comparison to cells treated with mock vehicle (blue, decreased; red, enriched). (G). Long-termed proliferation of KDM6A-silenced and non-targeted control (sgCtrl) MCF10A cells towards paclitaxel, AZD2014 and dasatinib. Cells were seeded in a 12-well plate and treated with indicated dose for 10 days. Media containing indicated inhibitors were replenished every 3 days. Mean ± S.D.; n=3; *p<0.05, **p<0.01. Experiments were repeated independently 2 times.

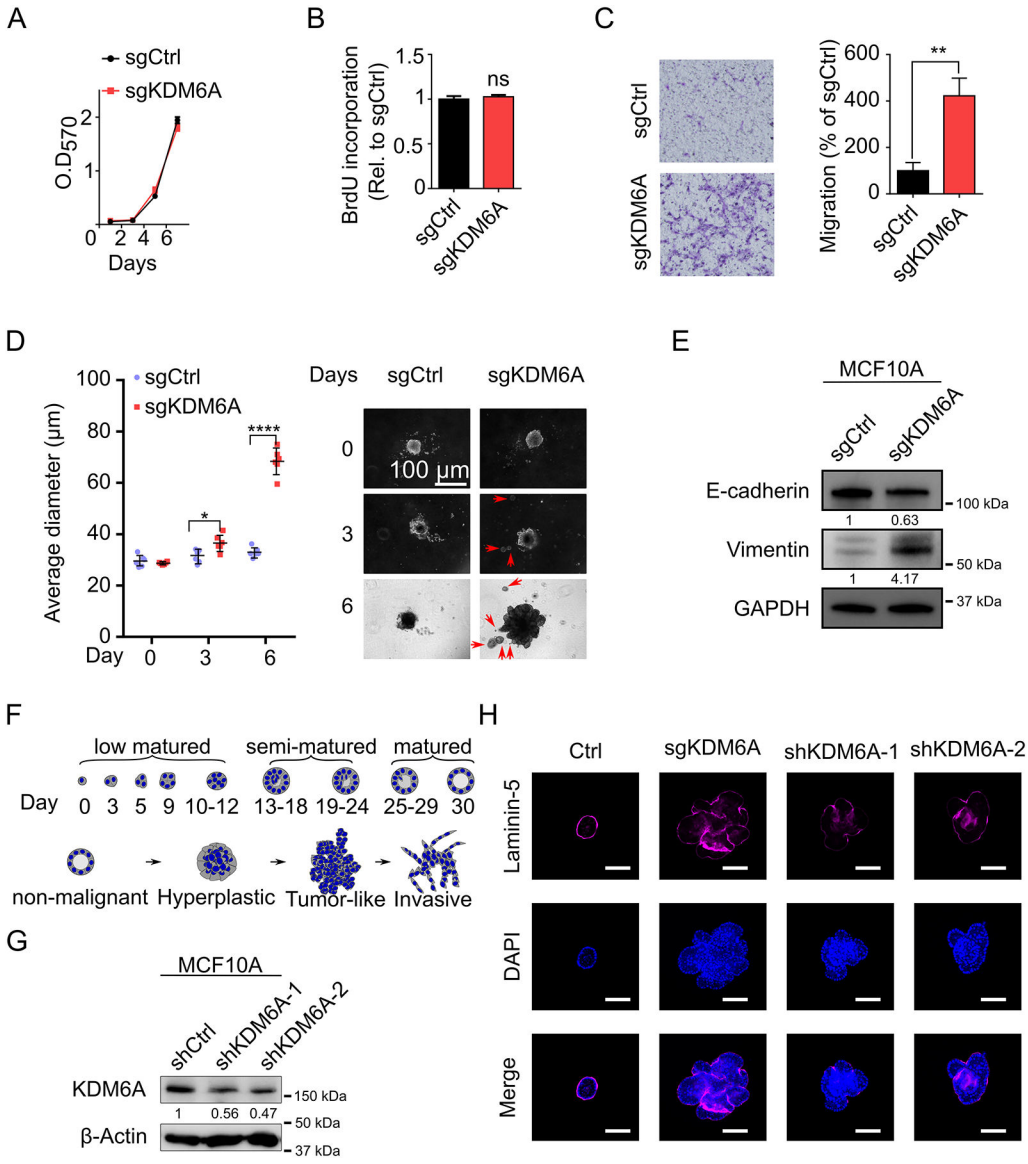

Figure 2. Silencing of KDM6A increased migration and induced a tumor-like transformation of MCF10A cells

(A). Cell growth (MTT assay) after CRISPR/Cas9 mediated silencing of *KDM6A* (sgKDM6A). sgCtrl, non-targeted sgRNA control. Mean ± S.D.; n=6. (B). BrdU assay measuring cellular proliferation. Mean ± S.D.; n=4; ns, statistical non-significance, student *t* test. (C). Left panel, representative image of migration of KDM6A-silenced and non-targeted sgRNA MCF10A cells in Boyden chamber assay; Right panel, quantitative measurement of migration. Mean ± S.D.; n=4; * *p<0.01, student *t* test. Migration assay was repeated twice. (D). 3D spheroid assay measuring capacities of invasion after silencing of KDM6A in comparison to control cells. Small spheroids around multicellular spheroids after incubation are indicated with red arrows. Mean ± S.D.; n=6; *p<0.05, ****p<0.0001, student *t* test. Scale bar=100 μm. Results are representative of three experiments. (E). Expression of E-cadherin and Vimentin after silencing of KDM6A in MCF10A cells. Normalized protein expression levels are shown under each band. (F) Cartoon displaying

normal acinar structure (upper) and acini at different stages of breast malignancy (lower). This cartoon was drawn in reference to previous publications[70–72]. MCF10A cells have the non-malignant feature of acinar structure. (G). Silencing of KDM6A expression with two different shRNAs (shKDM6A-1 and shKDM6A-2). shCtrl, non-targeted shRNA control. (H). Acini of MCF10A cells after silencing of KDM6A expression (sgKDM6A, shKDM6A-1 and shKDM6A-2). Control, wild-type MCF10A cells. Basal membranes were stained by Laminin-5 (pink), and nuclei were stained with DAPI (blue). Scale bar=100 μm. Acini assay was independently repeated 5 times.

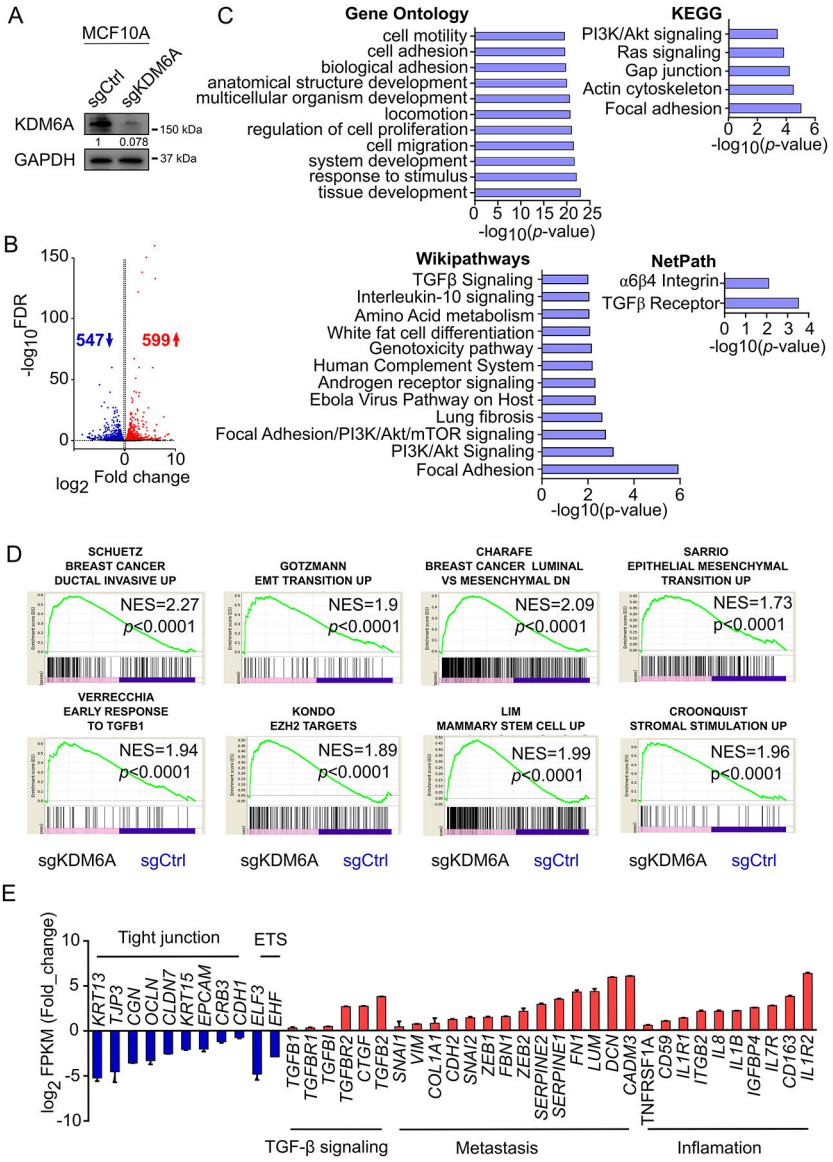

Figure 3. Silencing of KDM6A is linked to enrichment of TGF-β signature and cell migration and invasion pathways in MCF10A cells.

(A). Western blotting showing KDM6A expression in a single clone. sgCtrl, non-targeted sgRNA control; sgKDM6A, sgRNA targeting KDM6A. (B). Volcano plot showing significant upregulation of 599 genes and downregulation of 547 genes after silencing of KDM6A in MCF10A cells. Cut-off value for expression at X-axis is $\log_2$ Fold_change (sgKDM6A vs. sgCtrl) ≤ −0.58 or $\log_2$ Fold_change (sgKDM6A vs. sgCtrl) ≥ 0.58. For the Y-axis, the cut-off value is $-\log_{10}^{FDR} > 1$. (C). Gene ontology (GO), KEGG, Wikipathways and NetPath pathway analysis of the differentially expressed genes from KDM6A-silenced vs. non-targeted control. (D). Gene set enrichment analysis (GSEA) shows significantly enriched gene expression signatures in MCF10A cells after silencing of KDM6A. NES, normalized enrichment score. Statistical significance is shown by *p* value. (E). Expression levels of featuring genes involved in tight junction, ETS (erythroblast

transformation-specific), TGF-β signaling, metastasis and inflammation. Expression level is indicated with $\log_2^{FPKM(Fold\_change)}$ ± S.D.; n=2.

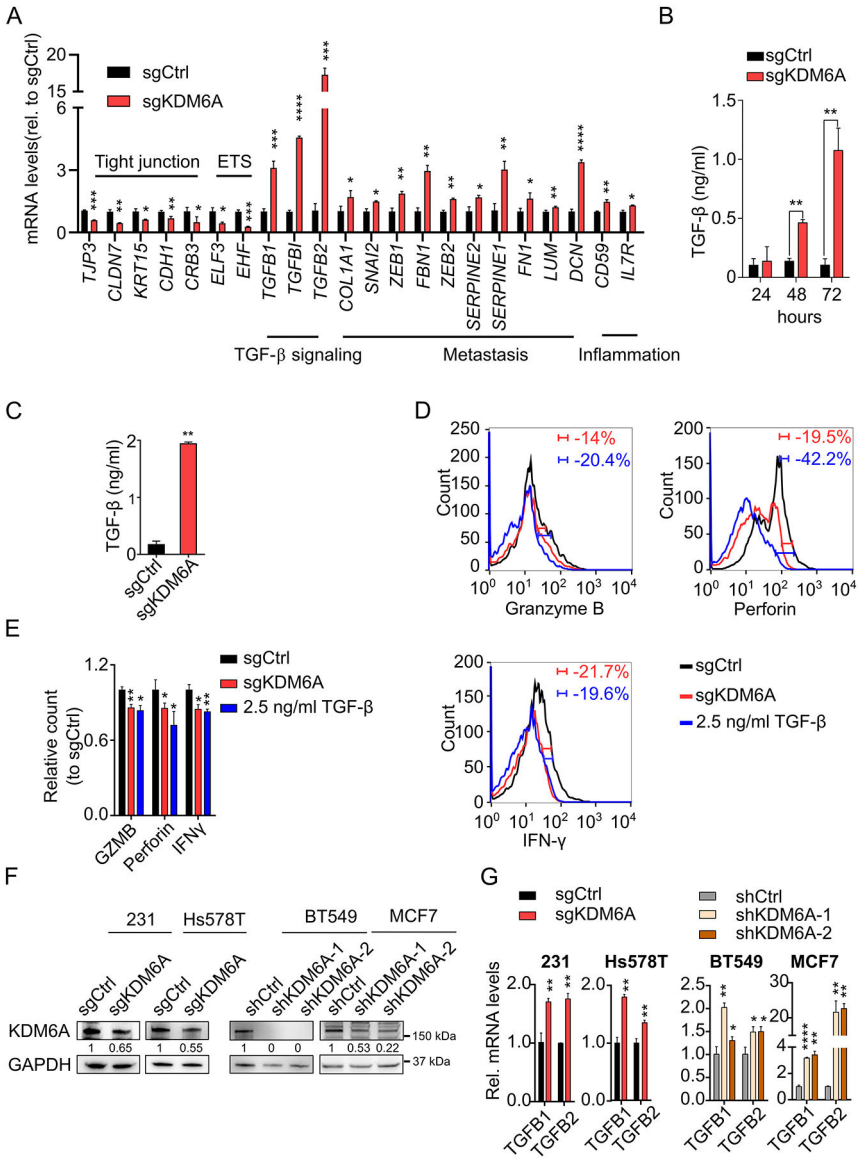

Figure 4. Extracellular secretion of TGF-β after silencing KDM6A and the effect on CD8+ T cells.

(A). qRT-PCR validation of expression of a panel of genes after silencing KDM6A expression, relative to non-targeted sgRNA control (Relative to sgCtrl). *GAPDH* served as internal control. Mean ± S.D.; n=3; **p*<0.05, ***p*<0.01, *** **p*<0.001, **** **p*<0.0001; student *t* test. (B). TGF-β expression in the culture media of either KDM6A-silenced (sgKDM6A) or control (sgCtrl) MCF10A cells (5×10^5 cells). Supernatants were collected after 24, 48 and 72 hours of incubation; Levels of TGF-β were examined by ELISA assay. Mean ±S.D.; n=3; ***p*<0.01; student *t* test. Experiments were independently repeated twice. (C). Summary of ELISA assays performed on secreted TGF-β with 1 million cells over 72 hours of incubation in serum free media. Mean ±S.D.; n=3; ***p*<0.01; student *t* test. (D). Purified CD8+ T cells were treated with conditioned media from sgCtrl cells or sgKDM6A cells examined in (C), or 2.5 ng/ml TGF-β in serum-free medium. Expression of cytotoxic genes granzyme B, perforin and IFN-γ in CD8+ T cells was analyzed after

24 hours of incubation. Cells were stained by specific antibodies versus control IgG and then analyzed by flow cytometry. (E). Mean (3 times) expression for granzyme B, perforin and IFN-γ as examined in (D). Mean ± S.D.; n=3; *p<0.05, **p<0.01. (F). Silencing of KDM6A expression in breast cancer cells with either CRISPR sgRNA targeting KDM6A [MDA-MB-231 (231) and Hs578T cells] or shRNA targeting KDM6A (BT549 and MCF7 cells). Levels of shRNA downregulation on KDM6A were quantified and normalized with GAPDH. sgCtrl, non-targeted sgRNA; sgKDM6A, sgRNA targeting KDM6A; shCtrl, non-targeted shRNA; shKDM6A-1 and shKDM6A-2, two different shRNA targeting KDM6A. (G) mRNA expression levels of *TGFB1* and *TGFB2* in breast cancer cells after reducing KDM6A expression. Mean ±S.D.; n=3; *p<0.05, **p<0.01, ****p<0.0001.

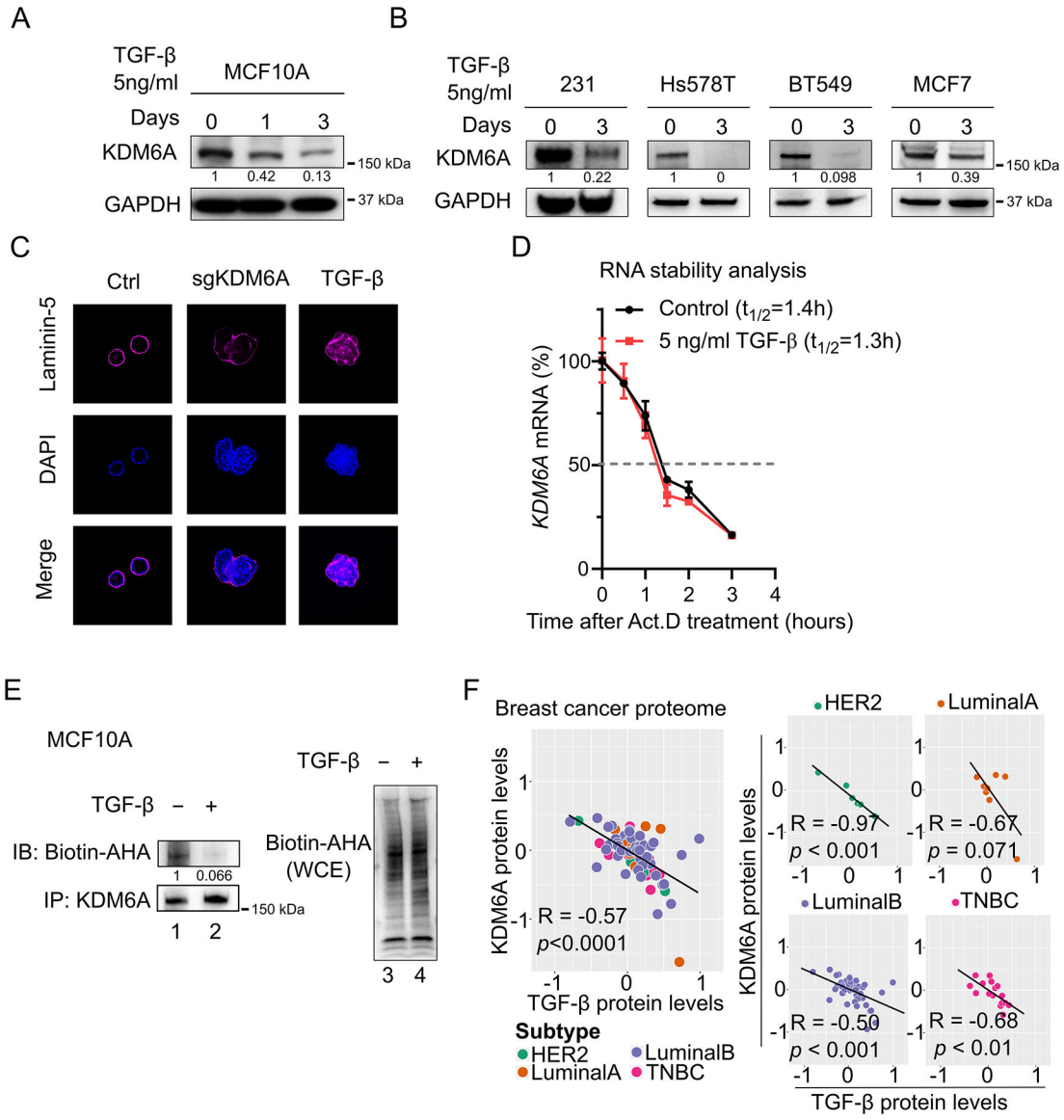

Figure 5. KDM6A translation is suppressed by TGF-β

(A). KDM6A expression in MCF10A cells after TGF-β (5 ng/ml) treatment for 1 and 3 days. (B). Reduced KDM6A expression was noted in MDA-MB-231 (231), Hs578T, BT549 and MCF7 breast cancer cells after treatment with TGF-β (5 ng/ml) for 3 days. (C) Acini of MCF10A cells in 3D culture showing tumor-like transformation after TGF-β treatment or CRISPR/Cas9-mediated silencing of KDM6A (sgKDM6A). Laminin-5 (pink) was stained for the basal membrane and nuclei were stained by DAPI (blue). Scale bar=100 μm. (D) KDM6A mRNA stability analysis. MCF10A cells were treated with 1.25 μg/ml Actinomycin-D (Act. D) after incubation with or without TGF-β for 72 hours. Levels of KDM6A mRNA are presented as % relative to the initial amount at time 0 when Actinomycin-D treatment began. (E) Analysis on *de novo* protein synthesis showed decreased KDM6A protein after TGF-β treatment. MCF10A cells were treated with or without 5 ng/ml TGF-β for 72 hours and cells were pulse-labeled with L-azidohomoalanine

(Biotin-AHA). KDM6A synthesis was examined by Biotin-AHA immunoblot of anti-KDM6A immunoprecipitations (lanes 1 and 2). Nascent synthesized KDM6A levels were quantified and normalized with total immunoprecipitated KDM6A. Examining bulk protein biosynthesis from whole cell extract (WCE) showed equal L-azidohomoalanine incorporation (lanes 3 and 4). (F). A strong negative correlation was noted between the protein expression level of TGF-β and KDM6A in breast cancer patient proteome data. Correlation of protein expression of TGF-β and KDM6A was also analyzed according to different molecular subtypes of breast cancer patients. Protein levels (z-scores) were measured with mass spectrometry by the Clinical Proteomic Tumor Analysis Consortium (CPTAC). Pearson's correlation, Fisher exact test.

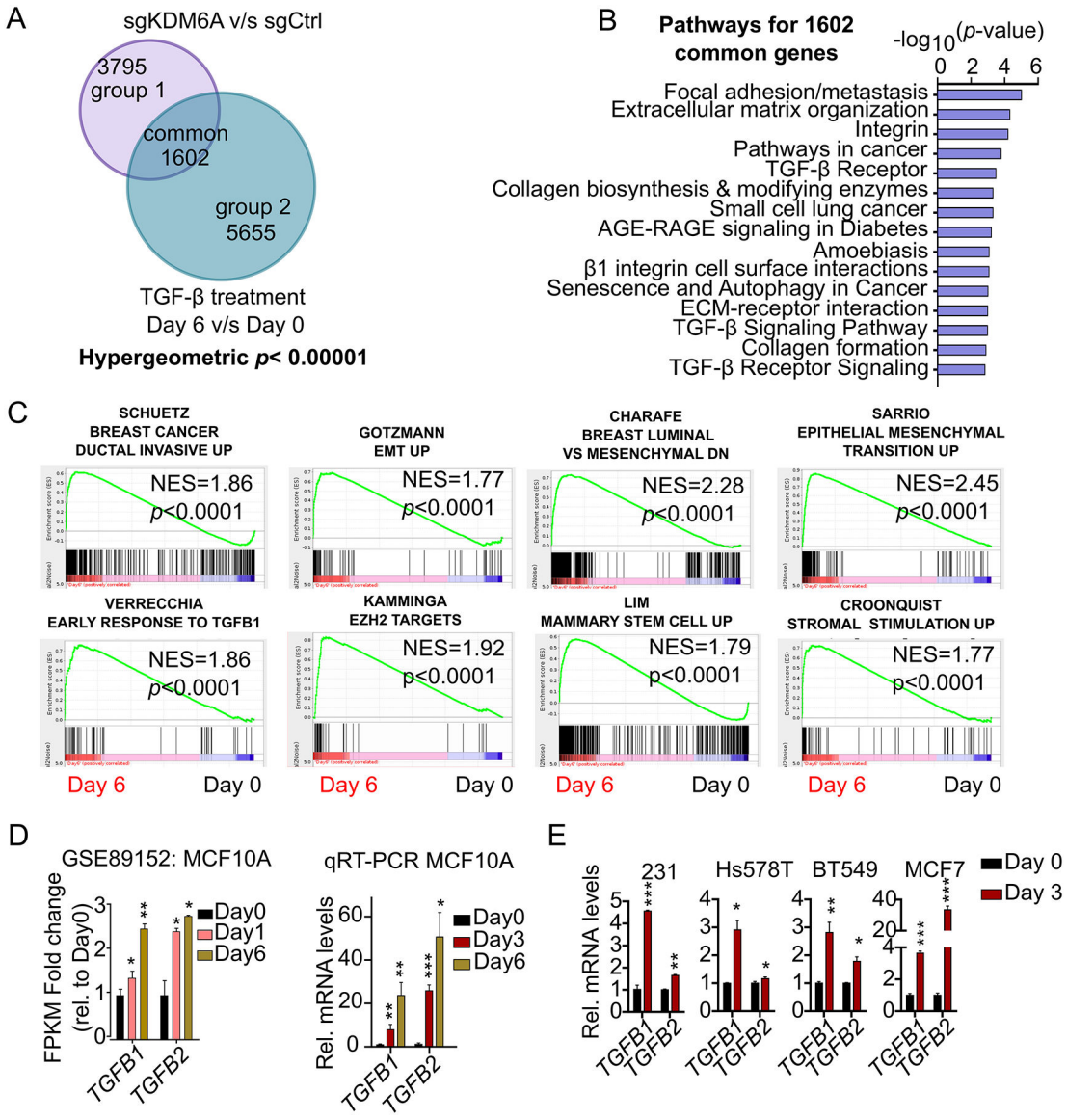

Figure 6. Signaling pathways were highly correlated between KDM6A-silenced and TGF-β-treated MCF10A cells.

(A). Venn diagram showing overlap of differentially expressed genes from RNA-seq data between KDM6A-silenced vs. non-target control (sgKDM6A vs. sgCtrl) and TGF-β-treated vs. untreated (GSE89152, 5 ng/ml TGF-β treatment Day_6 vs. Day_0) MCF10A cells. Cut-off value was set at $\log_2^{(\text{fold\_change})} \geq 0.45$ or $\log_2^{(\text{fold\_change})} \leq -0.45$. Significance of the overlap of differentially expressed genes from two RNA-seq datasets was calculated with hypergeometric tests. Group 1 indicates non-overlapping genes presented only in sgKDM6A vs. sgCtrl. Group 2 indicates genes presented only in TGF-β-treated vs. untreated data set. (B). Pathway analysis of 1,602 common differentially expressed genes from (A). (C). GSEA plots showing the enrichment of gene expression signatures of TGF-β-treated MCF10A cells. (D). TGF-β treatment (5 ng/ml) of MCF10A cells induced *TGFB1* and *TGFB2* mRNA expression in MCF10A cells. Mean ± S.D.; GSE89152, n=2; qRT-PCR, n=3; **p*<0.05, ***p*<0.01, ****p*<0.001; student *t* test. (E). After TGF-β (5 ng/ml) treatment for 3 days,

mRNA expression levels of *TGFB1* and *TGFB2* were also increased in MDA-MB-231, Hs578T, BT549 and MCF7 breast cancer cells, compared to untreated control cells (day 0). Mean ±S.D.; n=3; *$p<0.05$, **$p<0.01$, ***$p<0.001$; student *t* test.